Ambient radioactivity on a reconnaissance study tour of Bratislava – Dubai – Kathmandu – Nepal Himalaya

Andrej MOJZEŠ[1,*] ⓘD, Miroslav BIELIK[1,2] ⓘD, František MARKO[1] ⓘD,
Ján MADARÁS[2] ⓘD, Kamil FEKETE[2] ⓘD, Pavol SIMAN[2] ⓘD,
Juraj PAPČO[3] ⓘD, Ashok SIGDEL[4] ⓘD, Subash ACHARYA[4] ⓘD

[1] Comenius University, Faculty of Natural Sciences,
  Ilkovičova 6, SK-84215 Bratislava, Slovak Republic

[2] Slovak Academy of Sciences, Earth Science Institute,
  Dúbravská cesta 9, SK-84005 Bratislava, Slovak Republic

[3] Slovak University of Technology, Faculty of Civil Engineering,
  Radlinského 11, SK-81005 Bratislava, Slovak Republic

[4] Tribhuvan University, Central Department of Geology,
  Kirtipur, Kathmandu 44618, Nepal

Abstract: Ambient radioactivity originates mainly from natural sources and materials (rocks and soils, building and other man-made materials, and cosmic radiation), and less frequently from artificial radionuclides. A geoscientific comparative study of the geological structure of the Alpine-Carpathian and Himalayan mountain range systems primarily focused on the area of structure geology, tectonics, stratigraphy and petrology in connection with the in-situ sampling of magnetic susceptibility and radioactivity at rock outcrops was also utilized to perform continual monitoring and acquisition of the equivalent gamma dose rate values in the air of the surrounding environment. A Geiger-Müller dosimeter was used for continual recording at a sampling frequency of 2 minutes. Simultaneously, a data-logger was used to record the ambient temperature, humidity and pressure values at a sampling frequency of 4 minutes. The measurements cover the entire tour, in particular, Bratislava, Slovakia (42.5 hours) – flight (5.75 hours) – Dubai, United Arab Emirates (11.3 hours) – flight (4 hours) – Kathmandu, Nepal (12.2 days) – flight (4.8 hours) – Dubai (9 hours) – flight (6.25 hours) – Bratislava (48 hours) from 27 March 2019 to 15 April 2019. The levels of ambient radioactivity belonging to different environments are compared and discussed in the contribution. The differences are based on both the chemical composition of the geological basement and adequate building materials and the cosmic contribution. The results of the measurements show higher values of ambient radioactivity for the Nepal environments and lower values for Dubai, in comparison with Bratislava, and by far the highest, but safe values for international flights attributed to the high portion of cosmic radiation. The contribution was generated within the ambit of the research project APVV-16-0146 WECAFARE (WEstern CArpathians FAults

---

*corresponding author: e-mail: andrej.mojzes@uniba.sk

1. Introduction

The instrumental data collection of physical properties of the geological environment creates the core of geophysical measurements and significantly contributes to its more complete cognition. That is also true for the case of the Western Carpathians faults research project under the name "Multidisciplinary research of the geophysical and structural parameters and environmental impacts of the faults of the Western Carpathians". The international cooperation of experts and an effort to correlate and update knowledge led to the realization of a multidisciplinary geoscientific comparative study of the geological structure of the Alpine-Carpathian and Himalayan mountain systems in the form of an intensive 9-day field research stay in the area of Nepal Himalaya. A structure-geological, tectonic, stratigraphic and petrologic investigation was also accompanied by in-situ sampling of magnetic susceptibility and radioactivity at rock outcrops and by collecting the small-volume rock samples. Moreover, regarding radioactivity measurement issues, the so-called continual monitoring and recording of the equivalent gamma dose rate values in the air of the surrounding environment during the 20-day stay on the tour Bratislava (Slovakia) – Dubai (United Arab Emirates) – Kathmandu (Nepal) – Nepal Himalaya – Kathmandu – Dubai - Bratislava was carried out. The issues of the analysis of the radioactivity rock outcrops were thus enlarged by problems of background radioactivity and the contribution of cosmic radiation during the plane flights themselves. This article provides an evaluation and comparison between ambient radioactivity during the constituent trip periods.

2. Study aim

The goals of study were:
 – to carry out, as circumstances allowed, complete continual data collection

on radioactivity in the form of the equivalent gamma dose rate in the air
during the entire tour, together with the ambient temperature, humidity
and air pressure data;

– to process and evaluate such data in terms of their changes during the
  tour due to particular environmental differences;
– to compare the levels of ambient radioactivity and meteorological vari-
  ables between constituent tour stages; and
– to try to identify and distinguish the sources of the changes of the mea-
  sured variables during the tour.

The sources of the equivalent gamma dose rate in the air were natural
radionuclides present in the surroundings, either the geological or gener-
ally natural environs, or in man-made materials (building, technological
and other), where cosmic radiation presents a permanent contribution. To
a lesser extent, it is not possible to rule out the presence of artificial ra-
dioactive sources. This article does not include a detailed analysis of the
composition of radioactive sources (e.g. by the gamma-ray spectrometric
measurement) or an evaluation of the results of the detailed sampling of the
equivalent gamma dose rate at individual rock outcrops.

3. Methods and equipment

The continual measurements and data collection of the equivalent gamma
dose rate in the air were carried out by dosemeter based on the Geiger-Müller
detector at a recording frequency of 2 minutes. The GAMMA-SCOUT in-
strument with a registration and recording of gamma rays in an energy
range of 0.03–3 MeV was used for measurement purposes.

The continual measurement and data collection of the ambient air tem-
perature, humidity and pressure were carried out by the multifunction dat-
alogger VOLTCRAFT THP180 at a recording frequency of 4 minutes.

4. Study areas and their geological settings

The measurements were taken continuously at the above-mentioned record-
ing frequency on the Bratislava – Dubai – Kathmandu – Pokhara – Baglung
– Kalopani – Kagbeni – Muktinath – Tukuche – Beni – Pokhara – Kath-

mandu – Dubai – Bratislava tour from 27 March 2019 to 15 April 2019 (20 days). The reconnaissance study on the mentioned tour itself (Fig. 1) lasted 16 days from 29 March 2019 to 13 April 2019, and the direct field geological research in the Nepal Himalaya along the line of the Kathmandu – Pokhara – Baglung – Kalopani – Kagbeni – Muktinath – Tukuche – Beni – Pokhara – Kathmandu geological transect (Fig. 2) lasted 9 days from 1 April 2019 to 9 April 2019.

Due to the length of the planned field geological profile, i.e. approx. 200 km of the Kathmandu – Pokhara leg and approx. 175 km of the Pokhara – Muktinath leg, the field survey was performed with the help of 2 field cars (9-member research team) in the form of numerous stops at selected localities along with walking examinations of geological objects.

Fig. 1. Illustration of the entire tour in the Google Earth application.

In terms of covered distance, there were two different means of transportation: air transport comprising of 4 international flights (Bratislava – Dubai and Dubai – Kathmandu, Kathmandu – Dubai, Dubai – Bratislava) with large distances (thousands of kilometres) covered in a relatively short time (hours) and car + walking transport (in Bratislava, Dubai and Nepal) with short distances (up to hundreds of kilometres in Nepal) covered in a substantially long time (days). For this reason, the next short geological characterization is given for those tour parts covered by car and foot only, i.e. the Bratislava and Dubai areas and the field study trail in the Nepal
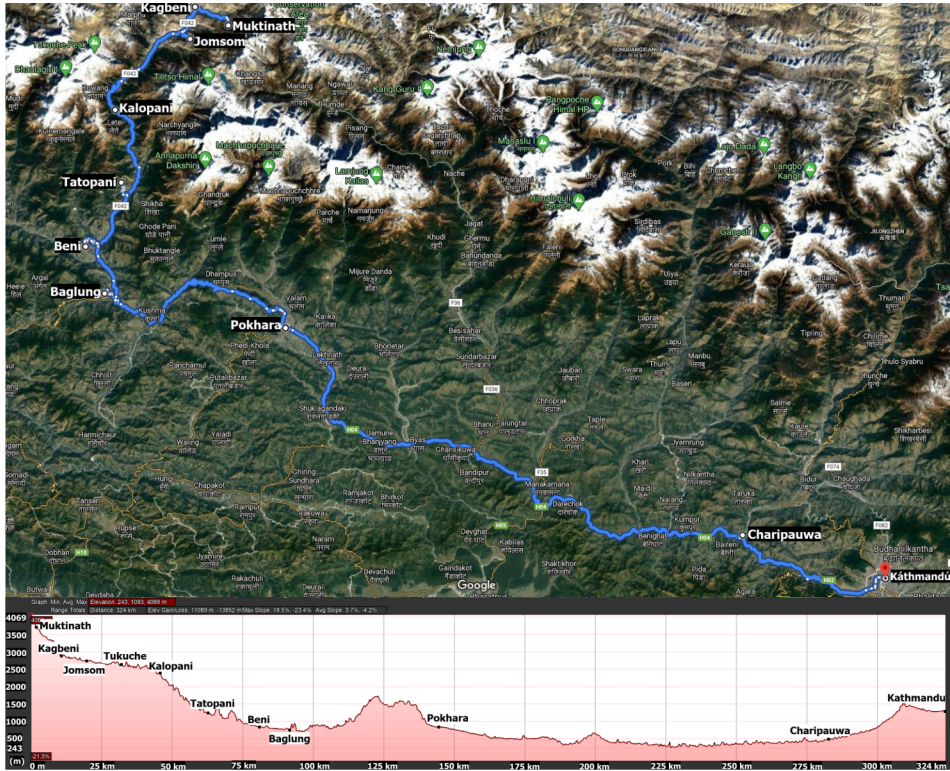
Fig. 2. Illustration of the field study geological transect (blue line) through the Nepal Himalaya and its height profile in the Google Maps and Google Earth applications.

Himalaya.

4.1. Bratislava (Slovakia)

The referred area of the eastern part of the city at the airport site is entirely comprised of Quaternary (the Late Pleistocene – Holocene) fluvial sediments (Fig. 3) in the form of lithofacially undivided alluvial clay soils and sandy to gravel soils (map index "fhh"), as well as sandy gravel and sand (map index "fš"). Postglacial deposits of alluvial sediments make up a substantial part of the fine-grained sedimentary surface cover of the sandy-gravel formation of the bottom accumulation of water flows (*Geological map of Slovakia 1:50 000, 2013*).
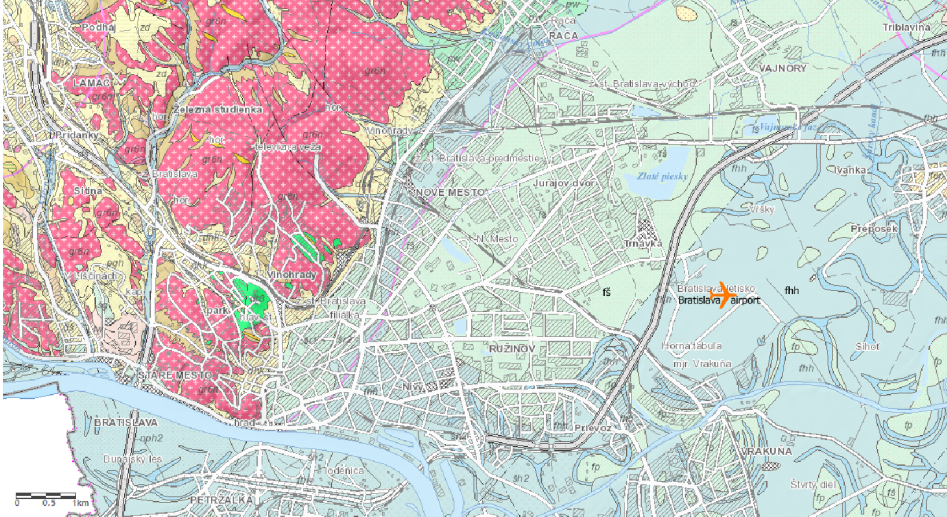
Fig. 3. Section of the geological map of the eastern part of Bratislava at the international airport localization (*Geological map of Slovakia 1:50 000, 2013*).

4.2. Dubai (United Arab Emirates)

The surface geology of the United Arab Emirates is concealed under a cover of sand (Fig. 4). Outcrops are confined only to the eastern part where the Oman Mountains form part of that region. The sands form dune ridges reaching heights of 150 m inland. Plain gravel areas – the so-called "desert floor", separate the dune ridges. Evaporatic flats (sabkha) dominate the coastal plains, which extend more than 80 km southwards into sand deserts. Consequently, the geology of this area is based exclusively on subsurface information (*Irani, 2001*).

Superficial deposits in the major urban areas in the emirates of Dubai, Sharjah and Ajman comprise the Quaternary fluvio-aeolian, aeolian and shallow marine deposits. Over much of the area, anthropogenic activity has resulted in the widespread deposition of made ground, including engineered fill. The Quaternary superficial deposits are underlain by variably calcareous and dolomitised sandstones, siltstones and conglomerates of the Barzaman Formation and weak mudstones, siltstones and gypsums of the Gachsaran Formation. In heavily urbanised areas, the extent of made

206

ground, the lack of exposure and the restricted nature of many of the site investigation reports means that the geological line-work was based on aerial photographs and satellite imagery taken prior to development (*Price et al.,* *2012*).
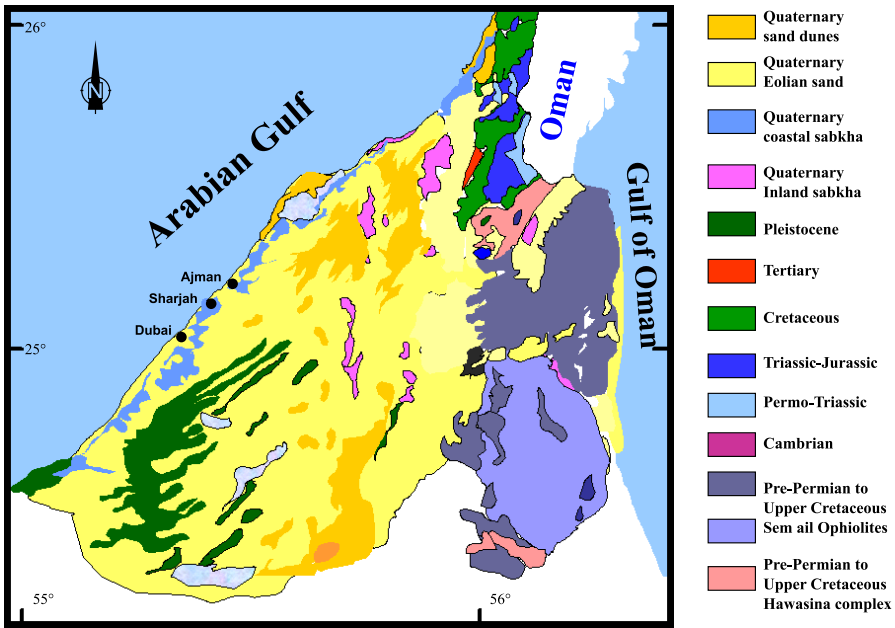
Fig. 4. Simplified geological map of the northern part of UAE (*Internet 1*, modified and *Internet 2*).

4.3. Kathmandu – Muktinath (Nepal)

The geological transect was very suitably selected considering the characteristic latitudinal features of the geological structure of Nepal with five fundamental NW–SE geological zones ranging from south to north in the following order: Terai and Bhabar Zone, Siwaliks and intermontane basins, Lesser Himalaya, Higher Himalaya and Tethys Himalaya (*Dhital, 2015*; Fig. 5). The first approximately 300 km-long part of the tour between Kathmandu and Beni followed a general NW–SE direction of geological units, which is why it runs mostly in the Lesser Himalaya zone, except for the first section – the approximately 70 km-wide Kathmandu surroundings with a compli-

cated geological structure of the Kathmandu Group belonging to the Higher
Himalaya zone (Figs. 5, 6a). The Lesser Himalaya is basically composed of
Proterozoic, mostly sedimentary (limestone, dolomite, shale and conglomer-
ates) and low-grade metamorphic rocks (quartzites, phyllites, slates). The
Kathmandu Group is composed mostly of Pre-Cambrian to Devonian meta-
morphic rocks (phyllites, micas and quartz schists, quartzites and sand-
stones) (Fig. 6b).
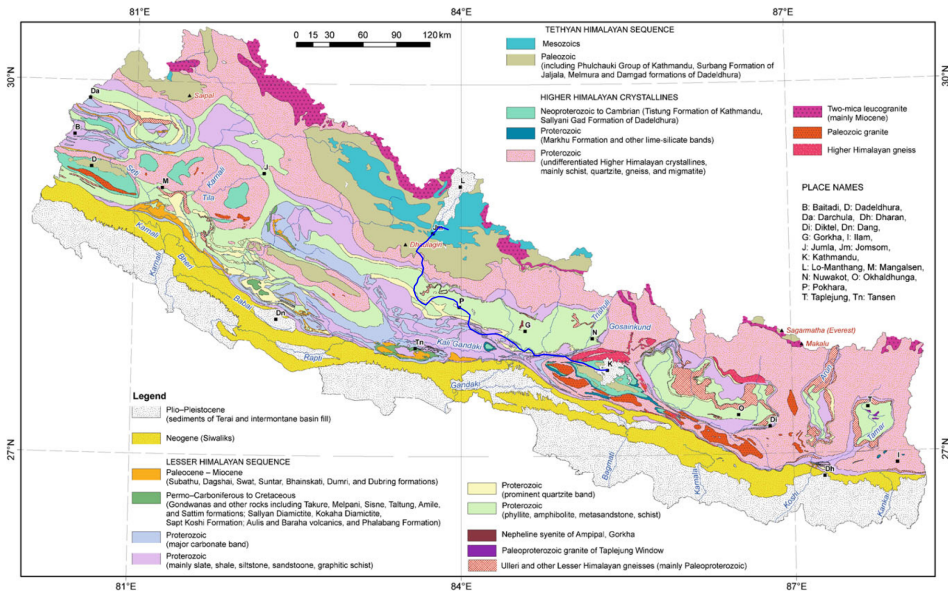
Fig. 5. Simplified geological map of Nepal (*Dhital, 2015*; supplemented by the blue line
of the geological transect).

The second part of the tour between Beni and Muktinath (around 112 km)
followed the Kali Gandaki River valley in a SSW–NNE direction across ge-
ological zones, and thus it cuts the Lesser Himalaya zone, the Main Central
Thrust (MCT), the Higher Himalaya zone, the fault South Tibetan Detach-
ment System (STDS) and ends in the Tethys zone (Muktinath) (Figs. 5,6a).
The Lesser Himalaya zone is, intersected by the tour approximately in the
part between Beni and Tatopani, and similar to the first part between Chari-
pauwa and Beni, it is mostly composed of the Proterozoic low-grade meta-
morphic rocks (quartzites, phyllites, carbonaceous slates) and sedimentary
rocks (green shales, compact dolomites, dolomitic limestones, sandstones

Fig. 6a. Section of the geological map of Nepal (*Himalayan Map House Pvt. Ltd., 2014*).

L E G E N D

Q — **QUATERNARY**
Alluvium boulders, gravels, sands and clays.

SIWALIK GROUP
(Mid-Miocene Pleistocene)

Us — **UPPER SIWALIK**
Coarse boulders, conglomerates with irregular beds and lenses of sandstones and thin intercalations of yellow, brown, grey sandy clays.

Ms — **MIDDLE SIWALIK**
Fine to medium grained, arkosic, pebbly sandstones with rare grey to dark grey clays and occasionally silty sandstones and conglomerates.

Medium to coarse grained friable arkosic sandstones and hard, compact massive sandstones intercalated with green to greenish grey clays, thin bands of pseudo-conglomerates and mudstones. Plant and animal fossils are present in clays.

Ls — **LOWER SIWALIK**
Fine grained, hard, grey sand stones interbedded with purple and chocolate coloured shales, noduler maroon clays and pseudo conglomerates.

SURKHET GROUP
(Cretaceous - Eocene)

Sn — **SUNTAR FORMATION**
Fine to medium grained, greenish grey sandstones and purple shales with intercalation of green splinnery shales.

Sw — **SWAT FORMATION**
Grey to dark grey, carbonaceous, shales with lenses of fine grained fossiliferous limestones (Nummulites śp, Assilina sp. etc.)

Mp — **MELPANI FORMATION**
White, grey, ferruginous well bedded massive or the quartzites interbedded with grey carbonaceous crumpled and redish brown shales and occasional conglomerates and fossiliferous limestones, Gastropodes (Promohildia), Pelcypods (Modiolo, Peuromya, Homomyol) and undreminable.

MID LAND GROUP
(Upper Pre-cambrian - Late Paleozoic)

GONDWANA SUB GROUP

Tk — **TAKURA FORMATION**
Black shales psammitic schists and conglomeratic phyllites

LAKHARPATA SUB GROUP

Lk Du / Rb — **LAKHARPATA FORMATION**
Fine grained, light blue, grey limestones and dolomites with thin intercalations of grey shales, white, pink dolomitic limestones, purple quartzites and green shales at the top. Algal structure and stromatotites are present.
Dunga quartzites beds.
Robang formation green chlorotic phyllites.
Layers of basic rocks.
Undifferentiated Lk, Sy, Sg, Gl

Sy — **SYANGJA FORMATION**
White pale orange pinkish or purplish calcarecus quartzites and quartzic limestones intercalated with dark grey purple and green shales strongly ripple marked quartzites at the base.

Sg — **SANGRAM FORMATION**
Black, dark grey to greenish grey shales with intercalation of limestones and quartzites.

Gl Ba — **GALYANG FORMATION**
Dark grey shales intercalated with thin grey calcareous slates and lamillae of carbonates. Thick beds of grey siliceous dolomites are found at place (Baitodi beds).

POKHARA SUB GROUP

Gp Cr — **GHAN POKHARA FORMATION**
Black to grey carbonaceous slates and green shales. Chour carbonates white to grey compact dolomite and dolomitic limestones interbedded with shales beds.

Nd — **NAUDANDA FORMATION**
White massive fine to medium grained quartzites with ripple marks interbedded with green phyllites. Basic intrusions are noted.

St — **SETI FORMATION**
Grey greenish grey gritty chlorite muscovite sandstones gritstones with conglomerates and white massive quartzites in the upper parts. Basic intrusions are noted.

DAILEKH SUB GROUP

Ks — **KUSHMA FORMATION**
Greenish grey White fine to medium grained at places ripple marked massive quartzite intercalated with green phyllites Basic intrusions are abundant.

Rm — **RANIMATTA FORMATION**
Grey greenish grey gritty phyllites gritstones with conglomerates and thin massive quartzites in the upper parts. Basic intrusions are abundant.

Ul — **ULLERI FORMATION**
Augen gneiss muscovite biotite gneisse feldspathic schists.

KATHMANDU GROUP
(Pre-Cambrian Devonian)

PHULCHOKI SUB GROUP

Ph — **PHULCHOKI FORMATION**
Light brown dolomite underlain by crinoidal limestones.

Ch — **CHITLANG FORMATION**
Dark slates with white quartzites at the base Impure limestones and two ferruginous beds containing trilobites.

Ca — **CHANDRAGIRI FORMATION**
Light fine grained crystalline limestones partly siliceous thick to massively bedded white quartzites in upper parts. Wavy limestones contain late ordovician schinoderms.

So — **SOPYANG FORMATION**
Dark argillaceous and many slates with thin limestones.

Ti — **TISTUNG FORMATION**
Dull green grey coloured phyllites pink purplish tinted sandstones with sandy limestones. Ripple marks, clay cracks, worm tracks are abundant pebbly beds near base.

BHIMPHEDI SUB GROUP

Mr — **MARKHU FORMATION**
Massive coarse to medium grained, crystalline marble changing northward to dark fine biotites schists interbedded with impure marbels and quartzites, stromatolites are found.

Sk — **SARUNG KHOLA FORMATION**
Fine grained dark green grey biotite and quartzitic mica schists occasionally garnetiferous interbedded with impure strongly micaceous quartzites.

Mk — **MAKSANG FORMATION**
White fine grained quartzites cross bedded.

Ta Pa — **TAWA KHOLA FORMATION**
Coarse grained dark grey garnetiferous muscovite biotite quartz schists interbedded with grayish impure quartzites pondrang quartzite member light green quartzites.

Ud — **UDAYAPUR FORMATION**
Coarse grained crystalline marbles with intercalations of schists.

Sp — **SHIPRING KHOLA FORMATION**
Coarse crystalline highly garnetiferous muscovite biotite quartz schists occasionally green chlorite schists at the base.

JALJALA GROUP
(Pre-Cambrian)

JALJALA SUB GROUP

Sb — **SURBANG FORMATION**
Grey to brown crystalline limestones interbedded with calc-schists calcareous schists and quartz-biotites schists.

Sr — **SIURI FORMATION**
Garnetiferous quartz-biotite schists and muscovite - biotite schists with calc schists quartzites and rare graphitic schists with blasto mylonitic augen gneiss of the base.

NAWAKOT GROUP

na — **NAWAKOT GROUP**
Precambrian to Lower Paleozoic. Mainly shallow marine sediments; lower part dominantly clastic (phyllites, sandstones, quartzites and calcareous sandstones). Stromatolitic limestones and black slates occur in the upper part. Basic sills and dykes present.

DADELDHURA GROUP
(Pre-Cambrian)

Sl — **SALLYANI GAD FORMATION**
Aplites, granite gneisses augen gneisses and biotite gneisses.

Kk Gh / Bu — **KALIKOT FORMATION**
Garnetiferous biotite schists and micaceous quartzites with gneisses.

Ghatte Gad Carbonates
Bluish crystalline limestones calcareous schists and quartz biotite schists.

Budhi Ganga Gneiss
Augen gneisses granitic gneisses and feldspathic schists.

Me — **MELMURA FORMATION**
Grey to dark grey phyllites quartzites and phyllitic schists.

Da — **DAMGAD FORMATION**
Grey to greenish grey quartzites calcareous quartzites and crystalline limestones.

Sl — **SALLYANI GAD**
Aplites granite gneisses augen gneisses and biotite gneisses.

HIMAL GROUP
(Pre-Cambrian)

Hm — **HIMAL GROUP**
Garnet biotite gneisses kyanite biotite gneisse garnetiferous mica schists augen gneisses micaceous quartzites and thin bands of marbles.

Mz — **TIBETAN SEDIMENTARY ZONE**
Mesozoic: Triassic to Lower Cretaceous. Mainly shallow continental platform sediments with local pro-delta facies in the Early Cretaceous. Sandstones, slates, shales with glauconite. Mainly ammonites and belemnites in Jurassic limestone.

Qh — **HIGHER HIMALAYA**
Pio-Pleistocene to Quaternary. Mainly fluvial and fluvio torrential sediments with local lacustrine clys and marlstones.

Tgr — **HIGHER HIMALAYAN CRYSTALLINES**
Tertiary (Miocene). Two mica leucocratic granites with tourmaline.

Pg — **PANGLEMA QUARTZITE**
Fine grained compact quartzitic schists and quartzites occasionally crystalline limestones.

Dk — **DWARE KHARKA SCHIST**
Medium to coarse grained quartz muscovite biotite schists garnetiferous schistose gneisses and kyanite schists.

Hg — **HIMAL GNEISS**
Two mica gneiss, granitic gneisses, banded gneisses, kyanite bearing gneisses and migmatites and thin bands of marbles.

Sh — Undifferentiated schists quartzites gneisses and calcareous silicate rocks (cs) of Bhimphedi Sub group and Tistung formation in various stages of migmatization.

Gn — Augen gneisses banded gneisses.

SYMBOLS

Biotite tourmaline granites

Syenites

Basic rocks

GEOLOGICAL FEATURES
STRUCTURES

⊢+⊣ Anticline axis   Thrust

⊢×⊣ Syncline Axis   ——— Fault

········· Geological Contacts

GENERALISED DIPS

$0°$ - $39°$

$40°$ - $69°$

$70°$ - $89°$

TOPOGRAPHIC FEATURES

International Boundary   River

Highway   Lake

Major, Minor Road   Bridge

Town/City   Peak

District Head Quarters   Pass

Fig. 6b. Legend of the geological map of Nepal (*Himalayan Map House Pvt. Ltd., 2014*).

and gritstones) (Fig. 6b). Generally, the grade of metamorphism increases from the foreland (south) to the hinterland (north) (*Dhital, 2015, p. 65*).

The Main Central Thrust (MCT) was intersected in the area of the village of Dana near Tatopani. This fundamental thrust structure repre-

sents the boundary between the underlying faintly metamorphosed Lesser Himalaya succession (south) and overlying Higher Himalayan crystallines (north) (*Dhital, 2015, p. 199*). The MCT comprises a wide zone of mylonitic rocks (fylonite) Proterozoic phyllites, quartzites and carbonates. The locally abundant presence of carbonate – quartzite veins and the remobilization of ferric oxides (limonitization), refers to fluid penetration in this zone. The increased seismicity, but also numerous natural thermal springs in the vicinity of the village of Tatopani (warm water in translation), also refer to recent activity of the tectonic zone.

The Higher Himalaya zone, between the villages of Tatopani and Kalopani, is composed of Proterozoic crystallines made up of medium to high-grade schists, quartzites and marbles together with augen and banded gneisses, migmatites and granites (*Dhital, 2015, p. 199*) (Fig. 6b). The Higher Himalayan crystallines are characterized by inverted metamorphism towards their base and a normal Barrovian type of metamorphism towards their top. The grade of metamorphism in the Higher Himalayan crystallines decreases progressively from the hinterland (north) towards the foreland (Siwaliks). Also, their metamorphic grade sharply diminishes towards the Tethyan sedimentary succession (*Dhital, 2015, p. 197*).

The Higher Himalayan crystallines are frequently truncated to the north by a system of normal faults called the South Tibetan Detachment System (STDS). This fault system was intersected in the area of the village of Kalopani. On the surface, the detachment is a discontinuous fault system with one or more splays. In some instances, it is represented by a shear zone (*Dhital, 2015, p. 197*). The South Tibetan Detachment System separates the medium to high-grade metamorphic rock of the Higher Himalaya from an overlying sedimentary or low-grade metamorphic secession of the Tethys Himalaya.

The last, most remote part of the tour between Kalopani – Jomsom – Kagbeni – Muktinath was in the Tethys Himalaya zone. The Tethyan Himalayan sequence mainly occupies the south periphery of the windswept Tibetan Plateau. The Tethyan rocks are made up of a variety of terrigenous and carbonate sediments, such as sandstones, siltstones, dolomites, limestones and shales (Fig. 6b). They range in age from Cambrian to Eocene. They are strongly folded and faulted, but conformably overlie the Proterozoic succession of the Higher Himalaya. Their grade of metamor-

phism generally increases from west to east. The Tethyan sediments have lateral changes and strong facies differences. The rocks are intricately folded and frequently verging due north, that is, opposite to the Higher and Lesser Himalayan successions. There are few Paleozoic remnants on top of the Higher Himalayan rocks (*Dhital, 2015, p. 285*).

5. Results and discussion

5.1. Overview

The results of the parallel recording of temperature, humidity and pressure of atmospheric air are presented in Fig. 7, while the overall results of ambient radioactivity recording on the Bratislava – Dubai – Nepal – Dubai – Bratislava reconnaissance study tour in the form of the equivalent gamma dose rate in the air from 27 March 2019 to 15 April 2019 are presented in Fig. 8. The graphs of the measured variables are presented in a time course, not a distance course. The changes in single variable courses are evident and easily readable in both figures and considering the fact that the path of the trips from Bratislava to Muktinath and back was almost identical; the curves are characterized by an almost mirror image with the centre in the most remote point of the tour – the Muktinath monastery and trekking ascent to the altitude of 4100 m a.s.l. in the Annapurna massif. This fact illustrates the satisfactory sensitivity of the instruments, the repeatability of their measurements and the stability of the meteorological conditions during the entire tour.

5.2. Meteorological parameters

From among the meteorological variables (Fig. 7), barometric pressure bears the highest information value as temperature and humidity were often influenced by the datalogger placement in baggage, the means of transportation or the indoor environment in dwellings.

The overall barometric pressure course (Fig. 7) reliably documents the dependence on altitude. Although altitude was not recorded, the pressure curve shows an evident difference between the low-lying regions of Bratislava (around 130 m a.s.l.) and Dubai (around 15 m a.s.l.) and the mountainous areas of the Nepal Himalaya. Also, the periods of four international
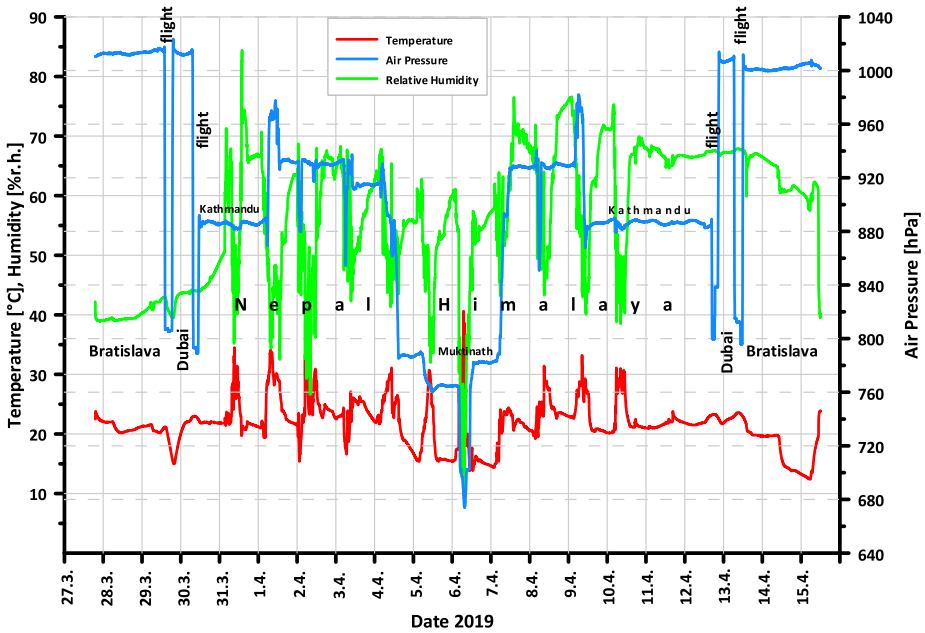
Fig. 7. Time course of meteorological parameters logged during the entire trip.

flights (Bratislava – Dubai, Dubai – Kathmandu and back) can be sharply distinguished, even if their expressive pressure minima at a flight altitude of about 10000 m a.s.l. has higher values than the lowest pressure minimum achieved during the trekking ascent to an altitude of 4100 m a.s.l. (in the middle of the curve in Fig. 7). This is due to overpressure conditions in the aircraft. Equally, there are easily identified areas in Nepal itself on the barometric pressure course (Figs. 7–9), e.g. the higher-lying Kathmandu plateau (around 1600 m a.s.l.), and the low-lying river valleys (around 300 m a.s.l.) on the road leading from Kathmandu to Pokhara, as well as the depression at Pokhara itself (around 1000 m a.s.l.) and the nearby lake (Fig. 2). From there, the gradual ascent follows up the Kali Gandaki River valley between the Dhaulagiri and the Annapurna massifs to the Muktinath monastery (around 3800 m a.s.l.) at the Upper Mustang border and to the altitude point of 4100 m a.s.l. below the Thorung La Pass (5416 m a.s.l.). The crossings of the deep valleys of the Trishuli and Marsyangdi rivers (around 300 m a.s.l.) on the road between Kathmandu and Pokhara, and the crossings of

mountain ranges, e.g. on the road between Pokhara and Baglung (around 1800 m a.s.l.) as well as the ascent to the Sarangkot observation hill (around 1590 m a.s.l.) near Pokhara are detected on the barometric pressure curve.

The basic statistical characteristics of the meteorological parameters for individual destinations and environments are presented in Table 1.

Table 1. Basic statistical characteristics of meteorological parameters for single destinations and environments.

	No. of measurements (à 4 min)	Minimum	Maximum	Mean	Standard deviation	Coefficient of variation
TEMPERATURE (°C)						
Bratislava (Slovakia)	1359	12.4	23.9	19.2	2.0	0.11
Dubai (United Arab Emirates)	321	15.0	22.9	21.2	1.5	0.07
Nepal	4750	13.8	40.6	22.3	3.8	0.17
aircraft flights	304	15.3	23.6	22.0	0.7	0.03
HUMIDITY (% r.h.)						
Bratislava (Slovakia)	1359	38.9	67.5	51.4	2.9	0.05
Dubai (United Arab Emirates)	321	39.5	67.5	55.2	0.7	0.02
Nepal	4750	9.8	84.4	58.1	10.6	0.18
aircraft flights	304	39.5	67.9	55.0	0.4	0.01
AIR PRESSURE (hPa)						
Bratislava (Slovakia)	1359	999.6	1017.8	1007.6	1.5	0.002
Dubai (United Arab Emirates)	321	1000.9	1023.6	1010.3	1.6	0.002
Nepal	4750	673.9	982.1	878.1	60.5	0.07
aircraft flights	304	788.9	1012.2	828.8	50.6	0.06

5.3. Equivalent gamma dose rate

The overall equivalent gamma dose rate course (Fig. 8) reflects changes in the ambient radioactivity of the studied destinations. Besides the natural gamma radiation of the surrounding geological and non-geological environment, its the most important component is the gamma component of cosmic radiation. These radioactivity components could not be separated by the

instruments that were used.

Based on the overall curve, it can be concluded that the lowest values of the equivalent gamma dose rate are connected with the Dubai environment, where they are bound to large complexes of the Quaternary sandy cover formations (*Price et al., 2012*), with the typically low content of radioactive elements (*IAEA, 1990*), as well as to the low contribution of cosmic radiation in consideration of the very low altitude of around 15 m a.s.l. (*IAEA, 1990*).

The higher values of the equivalent gamma dose rate are valid for the region of Bratislava near its airport. This area is composed of Quaternary clayey cover (*Geological map of Slovakia 1:50 000, 2013*) with a higher content of a generally more radioactive clay component (*IAEA, 1990*); but it also lies at a higher altitude (around 130 m a.s.l.), with an appropriately higher degree of cosmic radiation (*IAEA, 1990*) in comparison with Dubai.

Even higher values of the equivalent gamma dose rate were registered
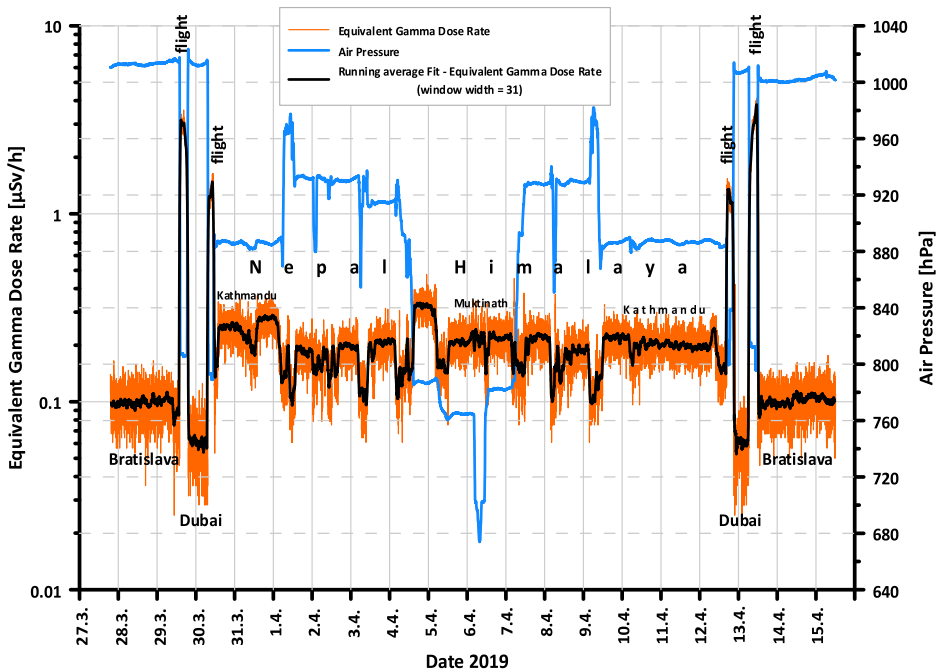
Fig. 8. Overview of the equivalent gamma dose rate and barometric pressure courses during the entire trip.

215

along the study transect through the Nepal Himalaya, where on one hand the surrounding mountain environment is comprised to a great extent by parent rocks and their fresh weathered cover with a possibly higher content of radionuclides, while on the other hand the contribution of cosmic radiation is even higher as a result of the high average altitude (*IAEA, 1990*).

The highest values by far of the equivalent gamma dose rate were detected during four international aeroplane flights (Bratislava – Dubai, Dubai – Kathmandu and back) with the highest degree of cosmic radiation at altitudes of around 10000 m a.s.l.

The basic statistical characteristics of the equivalent gamma dose rate for individual destinations and environments are presented in Table 2.

Table 2. Basic statistical characteristics of the equivalent gamma dose rate for individual destinations and environments.

	No. of measure-ments (à 2 min)	Minimum (μSv/h)	Maximum (μSv/h)	Mean (μSv/h)	Standard deviation (μSv/h)	Coefficient of variation
Bratislava (Slovakia)	2 715	0.025	0.176	0.099	0.020	0.199
Dubai (United Arab Emirates)	637	0.025	0.097	0.061	0.022	0.349
Nepal	9 502	0.053	0.476	0.199	0.055	0.279
aircraft flights	611	0.057	4.126	1.733	0.745	0.419

5.4. International flights and the equivalent gamma dose rate

The highest values of the equivalent gamma dose rate were registered during four international flights as a result of the high contribution of cosmic radiation at flight altitudes of around 10000 m a.s.l. The detector was placed in the luggage compartment of aeroplane during the entire flight time. The maximum value (4.126 μSv/h) and average value (1.733 $\pm$ 0.745 μSv/h) of the equivalent gamma dose rate during flights (Table 2) comply with official data stated by aircraft crews for flights at altitudes of up to 16500 m (*EURADOS WG5, 2004*), monitored from 1992 to 2003, with an average value of 3.8 $\pm$ 0.8 μSv/h, the most frequent measured value of 2.5$\pm$0.5 μSv/h and the maximum value of 19.2 $\pm$ 12.4 μSv/h. The probable reason for the lower values in our case was the registration of gamma radiation only, while

in the case of the EURADOS study, the complex sun and galactic cosmic radiation was a subject of interest (*EURADOS WG5, 2004*). In terms of safety and protection against radiation, the mean value of the effective dose obtained during the overall flight time (20.8 hours) at the level of 0.036 mSv (1.733 μSv/h $\times$ 20.8 h $=$ 36 μSv $=$ 0.036 mSv) was absolutely safe as one would have to undergo at least 300 flight hours at altitudes of over 9144 m in the equatorial zone (*Beck et al., 2006*), where our flights were undertaken to achieve the limit of the annual effective dose valid for the population at the level of 1 mSv/year (*Council Directive 2013/59/EURATOM, 2014*).

5.5. The Nepal Himalaya environment

On the basis of a more detailed view of the time course of the equivalent gamma dose rate (Fig. 9) and the barometric pressure (Figs. 7, 9), it is possible to state that these variables also depict some environmental changes within transfers in the Nepal Himalaya area itself (Fig. 2).

Considering the fact that the measured variables are presented in a time course and not a distance course, the longer one stays in one place (usually in accommodations) form the more relatively stable parts, where the values oscillate around the mean value, while car transfers to other accommodation places, usually accompanied by short stops at geologically interesting localities and outcrops, appear as shorter parts of lowered and less stable values of the equivalent gamma dose rate.

Repeated stays in some places, e.g. in the Kathmandu and Pokhara regions (on the way there and back), show approximately the same levels of the equivalent gamma dose rate. It is more evident for the Pokhara area (on average 0.178 μSv/h on the way there versus 0.177 μSv/h on the way back), than for the Kathmandu area (on average 0.242 μSv/h on the way there versus 0.201 μSv/h on the way back), where the equivalent gamma dose rate values increased significantly (up to 0.375 μSv/h) during the first stay during and after a strong thunderstorm on 31 March 2019 as a result of radon gas washing from the atmosphere to the earth's surface (Fig. 9). This rainstorm is documented by the highest measured values of air humidity (up to 84.4% r.h.) during the entire trip (Fig. 7). This was the only single, unstable meteorological event during the entire trip. The well-marked decrease of the equivalent gamma dose rate values immediately before the storm (to

the level of 0.115 μSv/h) was probably caused by the composition of building material in the vicinity of Durbar Square in the centre of Kathmandu (Fig. 9). The higher average values of the equivalent gamma dose rate in the Kathmandu region (0.222 μSv/h) in comparison with the Pokhara region (0.178 μSv/h) could have been due to the commonly higher radioactivity of the Pre-Cambrian to Devonian metamorphites (phyllites and shales) of the Higher Himalaya's Kathmandu Group, while the Pokhara area is comprised of Proterozoic, mostly sedimentary rocks (limestones, dolomites) and low-grade metamorphed rocks (quartzites) of the Lesser Himalaya sequences, with commonly low radioactivity.
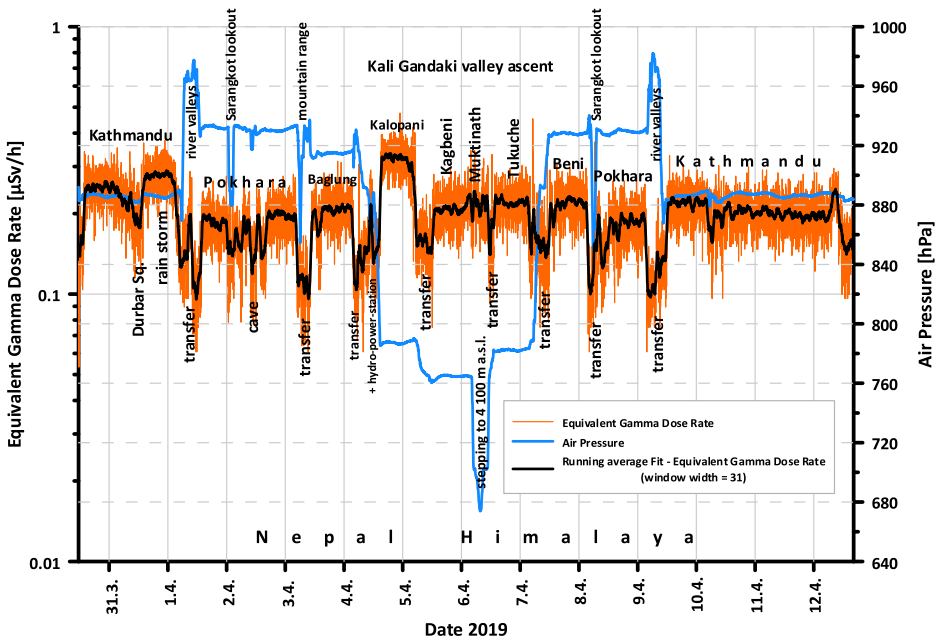
Fig. 9. Time courses of the equivalent gamma dose rate and barometric pressure in detail for the Nepal Himalaya part.

The transfer from the Kathmandu plateau to the Pokhara depression and back is indicated by short but distinct decreases in barometric pressure values (Figs. 7–9) when crossing the mountain range encircling Kathmandu, followed by stages of expressive increases in barometric pressure values when travelling along the deep valleys of the Trishuli, Marsyangdi and Seti Rivers

on the way to Pokhara.

In a similar way, due to the sharp minima of barometric pressure (Figs. 7–9), the ascents to Sarangkot lookout hill site (1590 m a.s.l.) in the Pokhara area, as well as the crossings of the mountain range on the way from Pokhara to Baglung (around 1800 m a.s.l.) are also indicated.

Starting from Pokhara, a sequential decrease of barometric pressure is recorded in connection with the gradual ascent following the Kali Gandaki River valley between the Dhaulagiri and the Annapurna massifs up to its lowest value of 673.85 hPa at the highest point – the Muktinath monastery (around 3800 m a.s.l.) and the altitude of 4100 m a.s.l. below the Thorung La Pass (5416 m a.s.l.).

The Baglung surroundings are also comprised of rock sequences of the Lesser Himalaya zone with an average equivalent gamma dose rate value (0.202 μSv/h) near the Pokhara area.

The section of lower equivalent gamma dose rate values (on average 0.145 μSv/h), belonging to the transfer from Baglung to Kalopani, contains a peak of higher values (on average 0.291 μSv/h) obtained during the guided tour of the inflow underground tunnel of the hydroelectric power station of the Mistri Khola Hydroelectric Project.

After crossing the Main Central Thrust (MCT) zone in the area of the village of Dana (Figs. 2 and 6a) the geological surroundings are formed by the Neo-Proterozoic rocks of the Higher Himalaya zone, which are represented by mica-schists alternating with banded gneisses, migmatites and granites showing the highest equivalent gamma dose rate values (maximally up to 0.476 μSv/h, on average 0.343 μSv/h) in the section of the villages of Tatopani, Dana and Kalopani.

After crossing the tectonic boundary of the South Tibetan Detachment System (STDS) between the villages of Kalopani and Larjung, the Tethyan Himalayan sequence of terrigenous and carbonate sediments such as sandstones, siltstones, dolomites, limestones and shales starts and continues further to the north. These rocks form the highest mountain peaks in the surroundings (Dhaulagiri – 8167 m a.s.l., Tukuche Peak – 6920 m a.s.l., Annapurna – 8091 m a.s.l., Nilgiri – 7061 m a.s.l., Tilicho Peak – 7134 m a.s.l. and others). The most remote points of the tour – the Muktinath monastery and the mountain stepping to 4100 m a.s.l. also lay in this geological environment. Sedimentary rocks show lower values of the dose equivalent rate

in the Kagbeni area (on average $0.210\,\mu\text{Sv/h}$) and Muktinath (on average $0.223\,\mu\text{Sv/h}$) as well as in the Tukuche area (on average $0.221\,\mu\text{Sv/h}$) on the way back from Muktinath.

The part with the highest measured equivalent gamma dose rate values (Kalopani – Dana – Tatopani) of the Higher Himalaya rocks did not show higher values on the way back. This was probably due to the fast vehicle transport, despite the fact that the short measurements at orthogneiss outcrops showed high equivalent gamma dose rate values (up to $0.453\,\mu\text{Sv/h}$).

The Beni area again formed by rock sequences of the Lesser Himalaya zone showed the same equivalent gamma dose rate values (on average $0.217\,\mu\text{Sv/h}$) as in nearby Baglung ($0.202\,\mu\text{Sv/h}$).

6. Conclusions

The recording measurements of ambient radioactivity in the form of the equivalent gamma dose rate in the air taken on the tour dedicated to the reconnaissance comparative study of the Alpine-Carpathian and Himalayan mountain range systems on the way from Bratislava (Slovakia) – Dubai (United Arab Emirates) – Kathmandu (Nepal) – Nepal Himalaya and back showed the presence of different equivalent gamma dose rate levels between particular destinations and environments and the possibility of the registration of their changes by the above-mentioned instruments. The differences were based on both the composition of the natural environment (geological and non-geological), and the varying contribution of cosmic radiation depending on altitude. The lowest registered equivalent gamma dose rate values were recorded in the Dubai environment (UAE); a higher equivalent gamma dose rate values were recorded in the Bratislava region (Slovakia) and even higher values of the entire study geological transect were recorded in the Nepal Himalaya environment. By far the highest equivalent gamma dose rate values were registered during the four international aeroplane flights at high altitudes; however, the effective dose value did not exceed the obligatory limits for safe exposure of the common population. The results confirm the generally known facts about the dependence of cosmic radiation growth on altitude increase, and the growth of geological environment radioactivity in the following sequence: sandy formations – clayey formations – weathered and non-weathered sequences of parent rocks.

References

Beck P., Bartlett D., Lindborg L., McAulay I., Schnuer K., Schraube H., Spurný F., 2006: Aircraft crew radiation workplaces: comparison of measured and calculated ambient dose equivalent rate data using the Eurados in-flight radiation database. Radiat. Prot. Dosim., **118**, 2, 182–189, `doi: 10.1093/rpd/ncl029`.

Council Directive 2013/59/EURATOM of 5 December 2013 stipulating the basic safety standards for protection against the dangers arising from exposure to ionising radiation. Official Journal of the European Union, L 13/1, 17. 1. 2014, 73 p.

Dhital M. R., 2015: Geology of the Nepal Himalaya. Springer, 498 p.

EURADOS WG5, 2004: Cosmic radiation exposure of aircraft crew. Compilation of measured and calculated data. Final report. Radiation Protection, Issue 140, Luxembourg, 271 p., online, available at `http://europe.eu.int`.

Geological map of Slovakia 1:50 000, 2013: State Geological Institute of Dionýz Štúr, Bratislava, online, available at `http://apl.geology.sk/gm50js` on 13. 1. 2020.

Himalayan Map House Pvt. Ltd., 2014: The Geological Map of Nepal, 1:1 000 000.

IAEA, 1990: The Use of Gamma Ray Data to Define the Natural Radiation Environment. IAEA-TECDOC-566, Vienna, 48 p.

Internet 1: Geology of Emirates. Available at `http://www.angelfire.com/az3/mohgameil/emirates.html` on 13. 1. 2020.

Internet 2: United Arab Emirates, Ministry of Energy and Industry, Geology and Mineral Resources Department: Geological Passport, Abu Dhabi. Available at `https://www.moei.gov.ae/assets/9ad782cf/geological_passport.aspx` on 13.1.2020.

Irani F. N., 2001: Geology of the United Arab Emirates. Schlumberger Drilling and Measurements, Abu Dhabi, 143 p.

Price S. J., Farrant A. R., Thomas R. J., Ellison R. A., 2012: Geology of the Dubai, Sharjah and Sir Bu N'Air 1:100 000 map sheet, 100–5, United Arab Emirates. Nottingham, UK, British Geological Survey, 54 p.